EVALUATION OF THE CORDEX-SEA MODELS PERFORMANCE IN SIMULATING CHARACTERISTICS OF WET SEASON IN INDONESIA

Alif Akbar Syafrianno[1, 2], Akhmad Faqih[1]*, Supari[2], Rini Hidayati[1]
[1]Department of Geophysics and Meteorology, Faculty of Mathematics and Natural Sciences, IPB University, Dramaga Campus, Bogor, Indonesia 16680
[2]Indonesia Agency for Meteorology, Climatology, and Geophysics, Jakarta, Indonesia
**E-mail: akhmadfa@apps.ipb.ac.id*

Article submitted: November 17, 2022 Article revised: March 10, 2023 Article accepted: March 10, 2023

ABSTRACT

Indonesia's climate is known to be challenging to adequately simulate by climate models because of the complexity of the weather system and sea-land distribution. Model evaluation is essential to measure confidence in the model results. This study evaluates the performance of the CORDEX-SEA model in simulating monthly rainfall patterns and the characteristics of seasonal rainfall, i.e., pattern, timing, length, and intensity, in Indonesia during 1986-2005. The performance of weighted (WMME) and unweighted ensemble methods are also calculated. Corrected CHIRPS data with similar seasonal patterns with point observation data is used as reference data to evaluate models. Percentage of the agreement of seasonal patterns between models and observation, FAR, and POD values were used to assess the model's ability to simulate seasonal patterns. WMME has the best seasonal patterns agreement with observation, 67% of all grids. The best model performance is shown by monsoonal patterns, with a POD value of 83% by WMME. Otherwise, all models could not describe an anti-monsoonal pattern, with a small POD (0-33%) and a high FAR (60-100%). In simulating the wet season on climatological, annual, and annual mean scales, both MMEs have similar performance and are better than individual models, with WMME performing best. However, on an annual scale, the yearly wet season produced by all models tends to approach its climatology value, making it less reliable in extreme years. Most models have higher daily and monthly rainfall than observation. In conclusion, the weighted ensemble method describes Indonesia's rainy season well, thus providing a reasonable basis for further research in climate projection analysis.

Keywords: CORDEX-SEA, model evaluation, wet season

1. Introduction

As a result of climate change, changes in the seasonal distribution of rainfall have been observed in parts of Indonesia [1]–[3] and are projected to continue in the future [4]. A shift in seasonal rainfall patterns would majorly impact livelihoods, infrastructure, agricultural output, and food security [5].

From several previous studies [6], [7], seasonal patterns in Indonesia can be categorized as follows: non-seasonal, areas with unclear differences between the wet season (WS) and the dry season; bimodal, areas with two WS occurring in one year; and unimodal, areas with one WS in one year. Unimodal areas can be further categorized as monsoonal and anti-monsoonal. Monsoonal areas have peak rainfall from December to February, while anti-monsoonal areas during May to July.

There are various methods to determine the onset and withdrawal of WS, for example, based on cumulative rainfall anomaly values [8]. However, this method can only be applied in unimodal areas. Therefore, Dunning et al. [9] extended that method to be applied to areas with twice WS in one year. This method is considered more suitable for use on model data because it does not use a definite threshold, so it does not need to be corrected for bias. Moreover, the calculation process is carried out differently for each point or *grid*.

A high-resolution model is needed to explain the characteristics of WS, which are influenced by large-scale and local climate factors [7]. Researchers use General Circulation Model (GCM) to understand future climate change [10], [11], but the low spatial resolution causes a lack of ability to represent atmospheric processes at a local scale [12], [13]. Currently available high-resolution projection data for the South East Asia region, namely the Coordinated Regional Downscaling Experiment – South East Asia (CORDEX-SEA), an aggregate of numerous dynamical downscaling outputs of various GCMs using multiple Regional Climate Models RCMs. From the output of CORDEX-SEA, several studies with the Southeast Asian domain have been carried out, for example: projections of extreme rainfall [14]; future changes in precipitation [5]; and the impact of climate change on sea level winds [15].

Climate models have various uncertainties, one of which comes from the parameters and structure of the model itself [16]. One of the solutions to reduce model uncertainty in simulating climatic conditions is to perform a multi-model ensemble, which has been done by previous researchers [17], [18]. Several methods for constructing ensemble models are by averaging directly without weighting [19] and with different weighting for each individual model [20].

In order to research projecting changes in seasonal characteristics in the future, it is important to know the performance of individual models and ensemble methods in the past period. Evaluation of the CORDEX-SEA model in simulating the timing and seasonal rainfall of WS in Southeast Asia has been carried out by Hariadi et al. [21], but did not test the model's ability to replicate unimodal/bimodal patterns. Research that tests the model's ability to simulate rain patterns (unimodal/bimodal) has never been done. This study aims to measure the ability of individual CORDEX-SEA models and their ensemble models (weighted and unweighted) to simulate seasonal rainfall characteristics (pattern, time, length, and intensity) in the reference period in unimodal and bimodal regions. The results of this study can be used as a basis for researching the projection of season characteristics in the future, especially in areas where the model can simulate rainfall patterns well.

2. Methods

Model data. This study uses daily rainfall data from the output of eight CORDEX-SEA simulation models (Table 1.) in the reference period of 1986-2005 following IPCC AR5 [22], which covers the territory of Indonesia. All model data have a spatial resolution of 0.25° x 0.25°, available in RCP4.5 and RCP8.5 scenarios [5].

Table 1. List of simulations used in this study.

Country	GCM (Developer Institute)	RCM (Developer Institute)
Vietnamese	CNRM-CM5 (CNRM, France)	RegCM4 [25] (ICTP, Italy)
Philippines	HadGEM2-ES (Hadley Centre, UK)	RegCM4 [25] (ICTP, Italy)
Thailand	MPI-ESM-MR (MPI-M, Germany)	RegCM4 [25] (ICTP, Italy)
Thailand	EC-Earth (EC-Earth consortium)	RegCM4 [25] (ICTP, Italy)
Indonesia	CSIRO MK3.6 (CSIRO, Australia)	RegCM4 [25] (ICTP, Italy)
South Korea	HadGEM2-AO (Hadley Centre, UK)	WRF [26] (NCAR USA)
Sweden	HadGEM2-ES (Hadley Centre, UK)	RCA4 [27] (SMHI, Sweden)
German	MPI-ESM-LR (MPI-M, Germany)	ROM4 [28] (MPI-M Germany)

Observation data. Daily rainfall data from The Climate Hazards group Infrared Precipitation with Stations (CHIRPS) [23], with a spatial resolution of 0.25° x 0.25°, are used as reference data to assess model performance. Corrections were made using dasarian rainfall data (10 days), blending between satellite data and in situ observation data used by BMKG, in order to bring the CHIRPS data closer to surface observation data. Considering day-i is in *dasarian-j* range, the ratio (r) of daily CHIRPS precipitation on day-i (PhC_i) with *dasarian* CHIRPS precipitation in *dasarian-j* (PdC_j) is calculated using Eq. (1). Correction Factor (CF) is then calculated using Eq. (2), with PdB_j is blended BMKG dasarian rainfall. The corrected CHIRPS dasarian rainfall is then obtained by Eq. (3), by adding CHIRPS daily rainfall with CF.

$$r = PhC_i / PdC_j \tag{1}$$

$$CF = r \times \left(PdB_j - PdC_j\right) \tag{2}$$

$$PhC\_k_i = PhC_i + CF \tag{3}$$

In addition, observational daily rainfall data from 98 BMKG stations that have been quality controlled [24] was used to compare the spatial pattern to the corrected CHIRPS data.

Multi-Model Ensemble (MME). This study uses two methods to calculate the ensemble value. First, the ensemble value is calculated based on the average value of all individual rainfall models without applying different weights. The resulting ensemble is referred to as SMME (Simple Multi-Model Ensemble). In the second method, the ensemble value is calculated based on the skill score (SS) [29] as a certain weight of each individual model, so it is called a Weighted Multi-Model Ensemble (WMME). Following Yang et al. [30], SS is calculated from the 3-month running average of monthly rainfall. Eq. (4) shows SS equation for each grid:

$$SS = \frac{4(1+CC)^4}{\left(NSD_m + \frac{1}{NSD_m}\right)^2 (1+CC_0)^4} \tag{4}$$

Where m is the individual model. NSD_m is the normalized standard deviation, namely the ratio between the standard deviation (SD) of the model and the SD of the observation. CC_0 is the maximum value of the correlation coefficient, which is 1. CC is the correlation coefficient between the observation and the model. The model performs best when the SS value is 1. The WMME rainfall data for each grid can be calculated by adding up the rainfall of the individual models multiplied by their SS values, then dividing by the sum of the SS values for each individual model.

Categorizing the seasonality. In categorizing an area as having a seasonal rainfall pattern or not, a combination of the Seasonal Index (SI) [31] and the method from Hamada et al. [6] is used. SI can be calculated by the Eq. (5).

$$SI = \frac{1}{R}\sum_{n=1}^{12}\left|X_n - \frac{R}{12}\right| \quad (5)$$

Where X_n is the monthly rainfall in the n^{th} month, and R is the annual rainfall. SI has a value from 0 (if monthly rainfall is the same throughout the year) to 1.83 (if all rainfall occurs in a month). A region is categorized as seasonal if SI>0.19.

Hamada et al. [6] define the seasonal rainfall pattern based on the difference between the maximum and minimum values of 3 running averages of climatological pentad rainfall. If the value is > 6mm/day, it is categorized as having a seasonal pattern and vice versa

This study categorizes an area as seasonal if it fulfills one of the above conditions. Using these two conditions produces a spatial pattern of areas with seasonal and non-seasonal rainfall that is more similar to the local climate zones used by BMKG (ZOM, *Zona Musim*), compared to using only one method.

Regions with seasonal rainfall patterns are then categorized as one (unimodal) or two (bimodal) WS in one year using harmonic analysis. The amplitude of the first (A_1) and second (A_2) components of the Fourier series based on daily rainfall data on each grid is calculated. An area is categorized as bimodal if $A_2/A_1 > 0.5$, and the length of the two climatological WSs is ≥ 28 days (referring to the BMKG, the minimum season length is three *dasarian,* and the shortest range of three *dasarian* is 28 days). The region will be categorized as unimodal if these conditions are not met. The method for determining climatological WS will be described in the next section. A similar method has been used for Africa [9] and Indonesia [6].

The unimodal area is again categorized based on the rainfall amount in a given month. An area is categorized as monsoonal if total rainfall from May to October is less than from November to March, similar to previous studies monsoonal pattern [6], [7]. Areas with higher total rainfall from September to February than from February to August are also monsoonal. The second criterion accommodates parts of Sumatra with slightly shifted rainfall peaks compared to the first monsoonal criterion. The unimodal region would otherwise be categorized as anti-monsoonal. This categorization is done to prevent the rainfall patterns of the monsoonal and anti-monsoonal zones from canceling each other out when the area is averaged for validation.

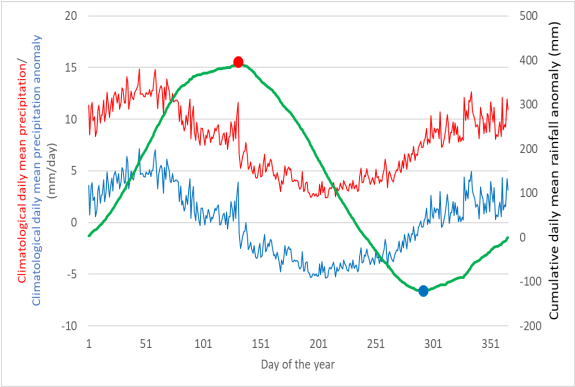

Figure 1. $C(d)$ (green line), Q_i (red line) and $Q_i - \bar{Q}$ (blue line) for points with a monsoonal pattern from WMME averaged over 1986-2005. The minimum (maximum) value of $C(d)$ is indicated by a blue (red) circle.

Determining onset and retreat of WS. In the unimodal region, the method from Liebmann et al. [8] in Dunning et al. [9] is used to determine WS's onset and retreat. The first step is to find the period when WS generally occurs in a year, called climatological WS. The climatological mean rainfall for each date, Q_i (i from 1 January to 31 December), and the climatological daily mean rainfall, $\bar{Q}$, were calculated. Then, the climatological cumulative daily rainfall anomaly on day d , C(d), is found:

$$C(d) = \sum_{i=1jan}^{d} Q_i - \bar{Q} \quad (6)$$

Where i starts from January 1 to the day d for which the calculation applies. The beginning of the climatological WS is marked by the day of the minimum value of $C(d)$, and the maximum value marks the end (d_e). An example of the calculation can be seen in Figure 1.

After determining the climatological WS, the next step is to find the onset and retreat of WS for each year by calculating the cumulative daily rainfall anomaly on day D, A(D):

$$A(D) = \sum_{j=d_s-50}^{D} R_j - \bar{Q} \quad (7)$$

Where R_j is the rainfall on day j, and A(D) is calculated every day from 50 days before d_s and after d_e. The day after the minimum in A(D) is the onset, and the day of the maximum (after the minimum) is the retreat date. Because WS can span years, the onset and retreat of WS in the first year are not counted. WS is considered absent if WS is less than 28 days long.

In the bimodal region, the onset and retreat of WS were determined using the method from Dunning et al. [9]. The climatological cumulative daily rainfall anomaly, C(d), is calculated similarly for the unimodal region. C(d) for each point is smoothed

using a 30-day moving average, called S(d). All values in S(d) that are more (less) than the four days before and after are considered as the maximum (minimum) value. All minimum values are considered as the onset of WS, and the first following maximum value is assumed to end that WS (Figure 2a). The two longest WS (Figure 2b) are considered as first climatological WS (d_{s1} to d_{e1}) and second WS (d_{s2} to d_{e2}).

The onset and retreat of the first WS (WS1) and the second WS (WS2) were then calculated for each year separately using the same method for the unimodal region. The calculations were performed over 20 days before and after d_s and d_e for each WS instead of the 50 days for the unimodal region.

Simple Daily Intensity Index (SDII). SDII [32] determines the average daily rainfall intensity during wet and dry seasons. Assume RR_{wj} is the daily rainfall on a rainy day, w (RR ≥ 1mm) in period j. If W is the number of rainy days in period j, with j from the beginning to the end of the WS, then:

$$SDII = \sum_{w=1}^{W} RR_{wj}/W \quad (8)$$

Validation method. The rainfall pattern for each grid across the dataset (observation and model) is determined. The Probability of Detection (POD) and False Alarm Ratio (FAR) are calculated for each rainfall pattern to measure the agreement of the rainfall pattern between the model and observation. For example, for the monsoonal pattern, assume a is the number of grids with a monsoonal pattern on the observation and the model, b is the number of grids with a monsoonal pattern on the model but has a pattern other than monsoonal on observation, and c is the number of grids with a monsoonal pattern on observation but has a pattern other than monsoonal in the model, the POD and FAR values can be calculated by the Eq. (9) and (10):

$$POD = a/(a+c) \quad (9)$$
$$FAR = b/(a+b) \quad (10)$$

By using rainfall patterns from observation data as rainfall patterns for all models, area-averaged rainfall for each rainfall pattern of each model is calculated. The WS onset, retreat, duration, and SDII were calculated for each rainfall pattern. Then these values are compared between observation and models. The Taylor diagram is used to analyze the correlation, standard deviation, and Centered Root Mean Square Difference (CRMSD) of monthly climatological rainfall between observation and models.

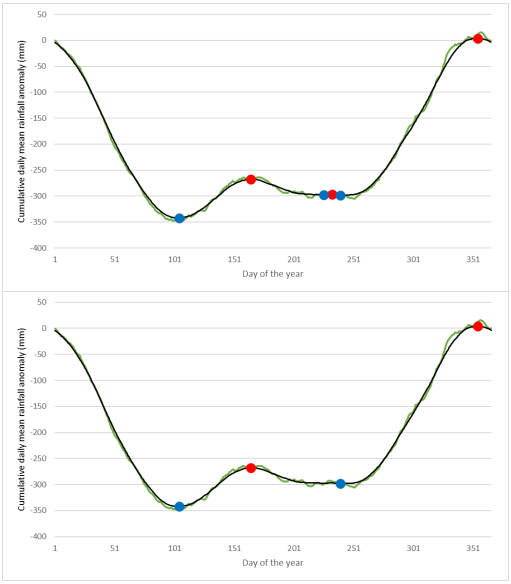

Figure 2. $C(d)$ (green) and $S(d)$ (black) for points with a bimodal pattern from WMME averaged over 1986-2005. a) the blue (red) dots show all the minimum (maximum) values of S(d). b) Two longest WS.

3. Result and Discussion

Rainfall patterns agreement. The rainfall patterns for each grid of the entire dataset, including observations, individual models, and ensemble models, can be seen in Figure 3. From the spatial rainfall patterns in the corrected CHIRPS data (Figure 3a) and observation stations (Figure 3d), it was possible to accurately depict the station point's rainfall pattern by making adjustments to the CHIRPS data. The suitability value between the model and the observation in describing seasonal patterns can be seen in Table 2. There are differences in the spatial distribution of seasonal patterns produced by the individual models. All individual models can simulate monsoonal patterns well, with a POD value of 42 - 89%. The most challenging rainfall pattern to be simulated by individual models is the anti-monsoonal pattern, with most models having a POD value of <13% and a high FAR of >90%. Some individual models produce anti-monsoonal patterns in the northern part of Sumatra, possibly due to differences in the wind patterns generated by the models in that region. The northern Sumatra region is known to have a different rainfall variability generation mechanism [33] which the model may not simulate well. Nonetheless, this hypothesis requires further investigation, which is beyond the scope of this study.

Compared to other individual models, the HadGEM2-ES (RCA4) model has the highest conformity with corrected CHIRPS (59%), as well as the best model in describing monsoonal patterns in terms of POD

values (89%). The CSIRO-MK3.6 (RegCM4) model best fits the bimodal pattern, with a POD of 69%. However, a high FAR value also follows it because CSIRO-MK3.6 (RegCM4) produces the broadest bimodal pattern compared to other individual models, which are evident on the islands of Sumatra and Kalimantan. The EC-Earth model (RegCM4) produced the most extensive anti-monsoonal pattern of any individual model and had the highest POD (33%). MPI-ESM-LR (ROM4) has the lowest total rainfall pattern conformity compared to other individual models.

WMME produces higher POD values than SMME in all rainfall patterns and higher total agreement. The POD values of WMME for all rainfall patterns are higher than most of the individual models. Although the highest POD values were obtained by different individual models for each seasonal rainfall pattern, WMME had the highest total agreement with corrected CHIRPS compared to all individual and SMME models. All models generally align with corrected CHIRPS in Java, Bali, NTB, NTT, and southern Papua. Rainfall pattern categories on the grid from the corrected CHIRPS data (Fig. 3a) were then used to define the regional rainfall mean for monsoonal, anti-monsoonal, and bimodal patterns from observation and model data. From now, corrected CHIRPS data will be referred to as observation.

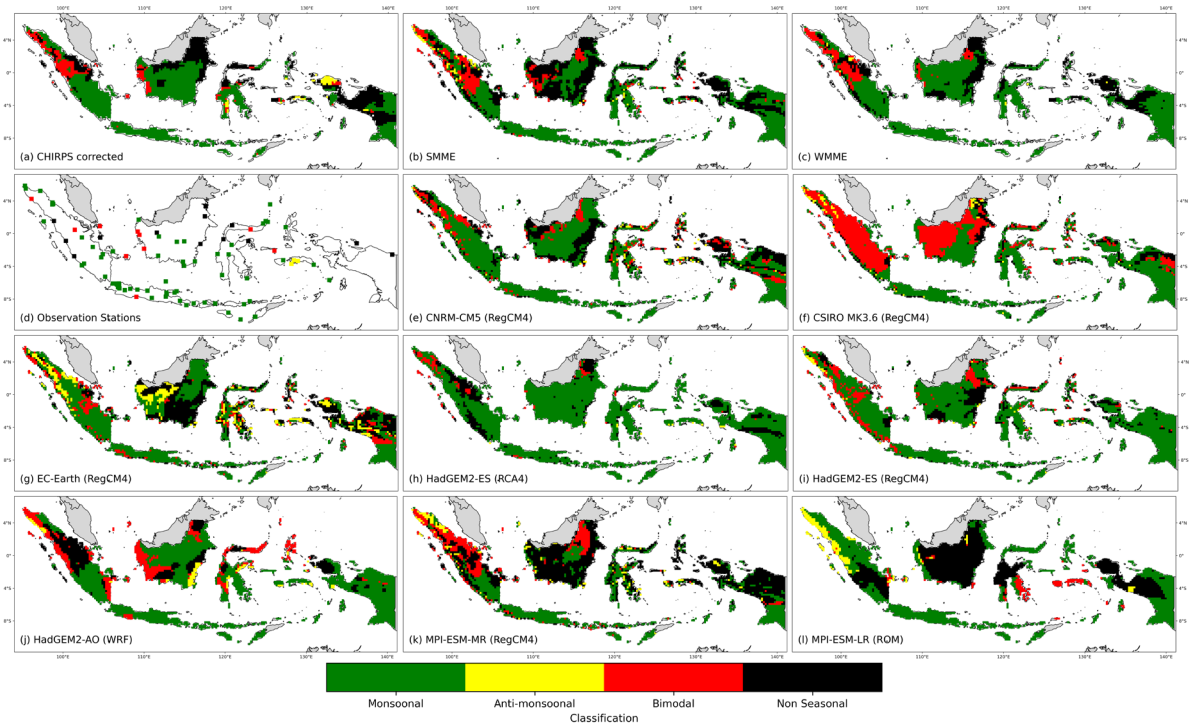

Figure 3. Classification of seasonal rainfall patterns from observations and models data.

Table 2. POD, FAR, and total agreement of rainfall pattern between observation with each model for each rainfall pattern. Values are presented in percent. The two best values are bold, with an * in the first best value.

Model	Monsoonal		Anti-monsoonal		bimodal		Total
	POD	far	POD	far	POD	far	Agreement
WMME	**83**	**25**	6	**77**	43	**53***	**67***
SMME	60	29	0	100	31	74	54
CNRM-CM5 (RegCM4)	74	31	4	94	24	81	55
CSIRO-MK3.6 (RegCM4)	56	33	0	100	**69***	84	45
EC-Earth (RegCM4)	56	33	**33***	94	12	88	45
HadGEM2-ES (RCA4)	**89***	37	4	**60***	12	**66**	**59**
HadGEM2-ES (RegCM4)	79	38	0	100	29	75	54
HadGEM2-AO (WRF)	73	31	7	93	**48**	72	56
MPI-ESM-MR (RegCM4)	42	**21***	**13**	94	31	80	46
MPI-ESM-LR (ROM4)	46	38	0	100	3	92	43

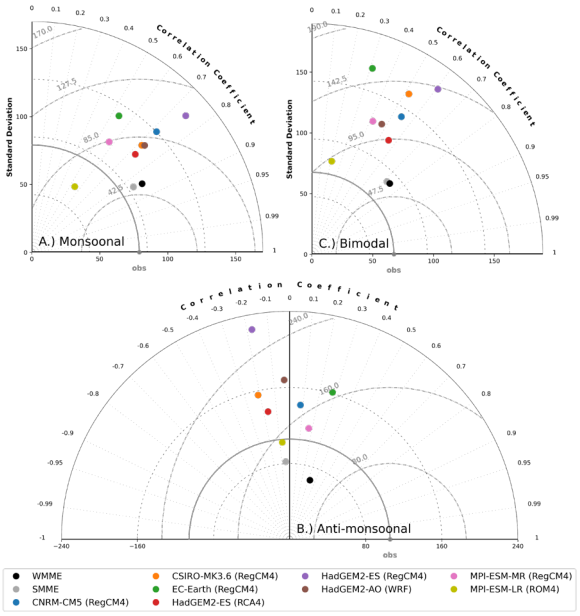

Figure 4. Taylor diagram for area-averaged monthly precipitation in regions a) monsoonal, b) anti-monsoonal, and c) bimodal. Small gray circles along the horizontal axis indicate observation data. The dashed line shows the STDEV. The dotted line shows the correlation between the models and the observation data. The CRMSD is indicated by the dash-dotted semi-circles about the observation point.

Performance of monthly rainfall. There are clear performance differences between rainfall patterns and between models in simulating monthly rainfall (Figure 4). In general, the individual and ensemble models can describe the monthly rainfall better in the monsoonal region, compared to other regions, with the models performing worst in the anti-monsoonal region. The low performance of the model on anti-monsoonal regions is due to the inability of the model to simulate anti-monsoonal patterns on observational data, as discussed in the previous sub-chapter. The model's poor performance in areas with anti-monsoonal patterns, which are mostly found on small islands, is in line with previous studies [5]. Compared to observational data in monsoonal areas, all individual models have a correlation value of 0.5-0.8 and Centered Root Mean Square Difference (CRMSD) <100 mm/month, while for STDEV, some individual models have values similar to observational data. In the anti-monsoonal region, all individual models had a correlation value of <0.3, even negative. The CRMSD values ranged from 100 to 250 mm/month, and the STDEV values differed greatly from the observation data. All individual models in the bimodal region have correlation values of 0.2-0.6, CRMSD values of 60 – 150 mm/month, and STDEV, which tends to differ from the observation data.

Application of MME from individual models resulted in better performance than all individual models in all regions, except for SMME in the anti-monsoonal region. The ensemble model correlation is > 0.8 in the monsoonal region and > 0.7 in the bimodal region. Both MMEs produce a similar performance on Taylor Diagram. Nevertheless, WMME's performance is better than SMME in all regions, as seen from the higher correlation value and lower CRMSD. However, the STDEV value of SMME is slightly closer to the observation data than WMME.

Performance of climatological WS. The pattern of the climatological cumulative daily rainfall anomaly for all seasonal rainfall patterns and all models can be seen in Figure 5. From the area-averaged rainfall of grids with monsoonal patterns (using the same grids as observation data), all individual models and MMEs can produce monsoonal patterns. From the climatological observation data, WS occurs from October 26 to May 12, with a duration of 200 days and SDII 9.1 mm/day. Differences in onset, retreat, duration, and SDII of WS from all models with observation can be seen in Figure 6. WS onset occurs earlier in all models than in observation, except HadGEM2-AO (WRF) and HadGEM2-ES (RCA4). All models produce a more diverse retreat of WS. All models produce higher SDII than the observation, except MPI-ESM-LR (ROM4). All MMEs produce similar WS lengths and are closer to observation than all individual models, with WMME being the best by one day difference from SMME.

Based on the area-averaged rainfall of grids with anti-monsoonal patterns, observation data show that climatological WS spans from April 25 to October 31 with a duration of 190 days and an SDII of 10.5 mm/day. Figure 5b shows that only two models produced an anti-monsoonal pattern on the same grids as observation. However, the onset, retreat, and duration of the climatological WS of the two models have a large difference from the observation data (Figure 7). The CNRM-CM5 (RegCM4) model simulated an earlier WS onset of up to two months, while the EC-Earth (RegCM4) simulated a longer duration of WS of up to 43 days. This is due to the models' inability to simulate correct rainfall patterns in grids with anti-monsoonal patterns from observation data, seen from the low POD in the previous sub-chapter. Thus, the anti-monsoonal pattern needs to be further validated on an annual scale.

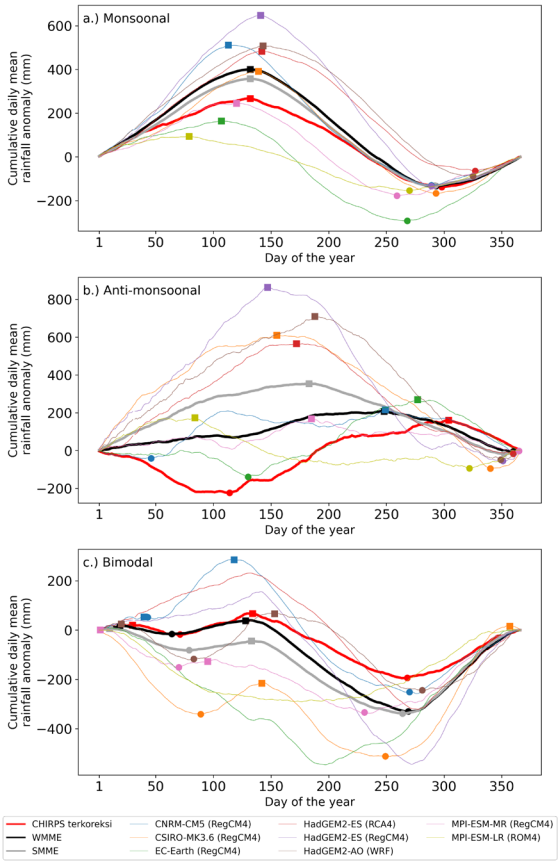

Figure 5. Cumulative daily mean rainfall anomaly for area-averaged data in regions a) monsoonal, b) anti-monsoonal, and c) bimodal. The circle (square) indicates the onset (retreat) of the climatological WS.

	SDII	Onset	Retreat	Duration
WMME	4.2	-5	0	5
SMME	5	-6	0	6
CNRM-CM5 (RegCM4)	6.6	-9	-19	-10
CSIRO-MK3.6 (RegCM4)	5.6	-5	7	12
EC-Earth (RegCM4)	8.8	-30	-25	5
HadGEM2-ES (RCA4)	2.4	29	10	-19
HadGEM2-ES (RegCM4)	8.7	-9	9	18
HadGEM2-AO (WRF)	5	27	11	-16
MPI-ESM-MR (RegCM4)	6.2	-39	-12	27
MPI-ESM-LR (ROM4)	-0.5	-28	-53	-25

Figure 6. Climatological WS difference between the model and observation in the monsoonal regions. Onset, retreat, and duration (SDII) are shown in days (mm/day).

	SDII	Onset	Retreat	Duration
CNRM-CM5 (RegCM4)	6.9	-68	-55	13
EC-Earth (RegCM4)	11.4	16	-27	-43

Figure 7. Same as Figure 6, but for the anti-monsoonal regions.

a) Bimodal WS1

	SDII	Onset	Retreat	Duration
WMME	4.4	-7	-6	1
SMME	6.1	8	-1	-9
CSIRO-MK3.6 (RegCM4)	7.3	-1	-39	-38
HadGEM2-AO (WRF)	8.8	12	19	7
MPI-ESM-MR (RegCM4)	7.4	18	8	-10

b) Bimodal WS2

	SDII	Onset	Retreat	Duration
WMME	6.2	1	-11	-12
SMME	8.1	-4	-20	-16
CSIRO-MK3.6 (RegCM4)	8.5	-37	-28	9
HadGEM2-AO (WRF)	8.5	13	-10	-23
MPI-ESM-MR (RegCM4)	9.6	-19	-38	-20

Figure 8. Same as Figure 6, but for the bimodal regions at a) WS1 and b) WS2.

Observation data show that climatological WS1 occurred from 13 March to 14 May with SDII of 8.7 mm/day in the bimodal region, while WS2 occurred from September 26 to January 30 with SDII of 9 mm/day (Figure 5c). The WS2 occurs longer, with a duration of 128 days, compared to the WS1, which occurs for 63 days. Both MMEs and three individual models could generate a bimodal pattern, with the differences shown in Figure 8. Compared to individual models, MMEs can produce more similar timing of the WS1 and the WS2 with the observation. Although the WS1 happened earlier when seen from the beginning and the end of the WS1, WMME had the closest WS length with observation in the WS1. WMME also produces the most similar WS2 with the observation. The SDII in both WSs produced by all models has a wet bias compared with observation, with WMME having the least bias. In general, climatological WS1 is better simulated by all models than climatological WS2. Besides being associated with the movement of the ITCZ [7], the WS in the bimodal region is also influenced by the monsoon system that occurs. WS1 coincides with the Asian Monsoon, and WS2 partially coincides with the Australian Monsoon. The higher wind bias during the Australian Monsoon compared to the Asian Monsoon [5] may be the reason why WS1 can be simulated more by the model than WS2.

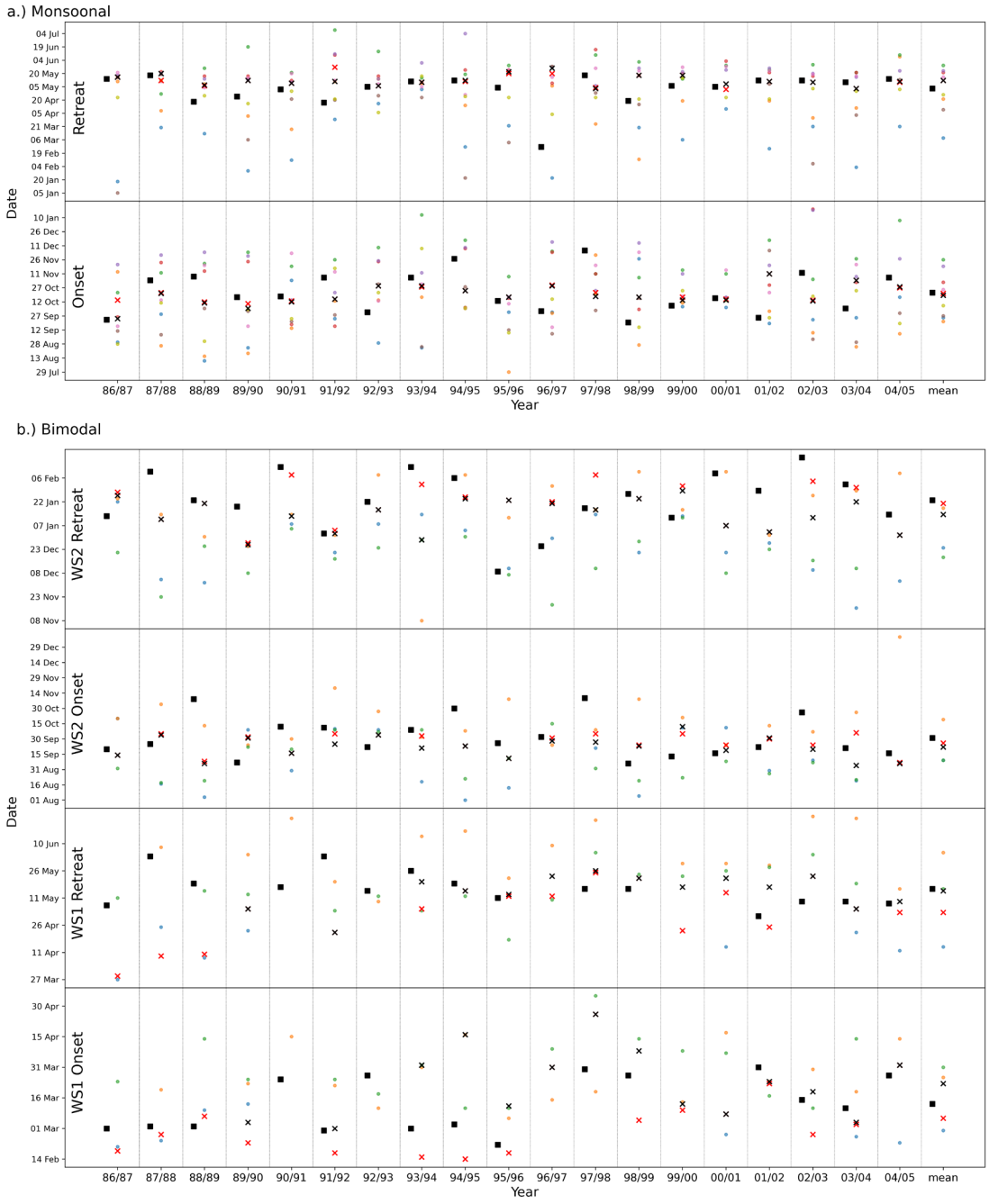

Figure 9. Interannual onset and retreat dates of the WS for regions a) monsoonal and b) bimodal.

Performance of annual WS. The annual WS cycle can be seen in Figure 9. From the observation data, the annual average of WS in the monsoonal region occurs from October 22 to May 2 with a duration of 193 days and an SDII of 9.3 mm/day. The onset of WS each year in the observation data is more diverse than the retreat of WS, which occur around the mean value. The individual models produce more varied WS onset and retreat than the two MMEs, which generally occur around the mean value. In years with extreme events, such as the strong El Nino in 1997-1998, observation data indicate an earlier end of the 1997 WS and a late onset of the 1998 WS. MMEs cannot simulate the impact of these extreme events, as shown by the onset and retreat of WS around its mean value. The MMEs averaging the values of all models with specific weights. As a result, the variation in values between individual models, including extreme values, will disappear, as stated in previous studies [34].

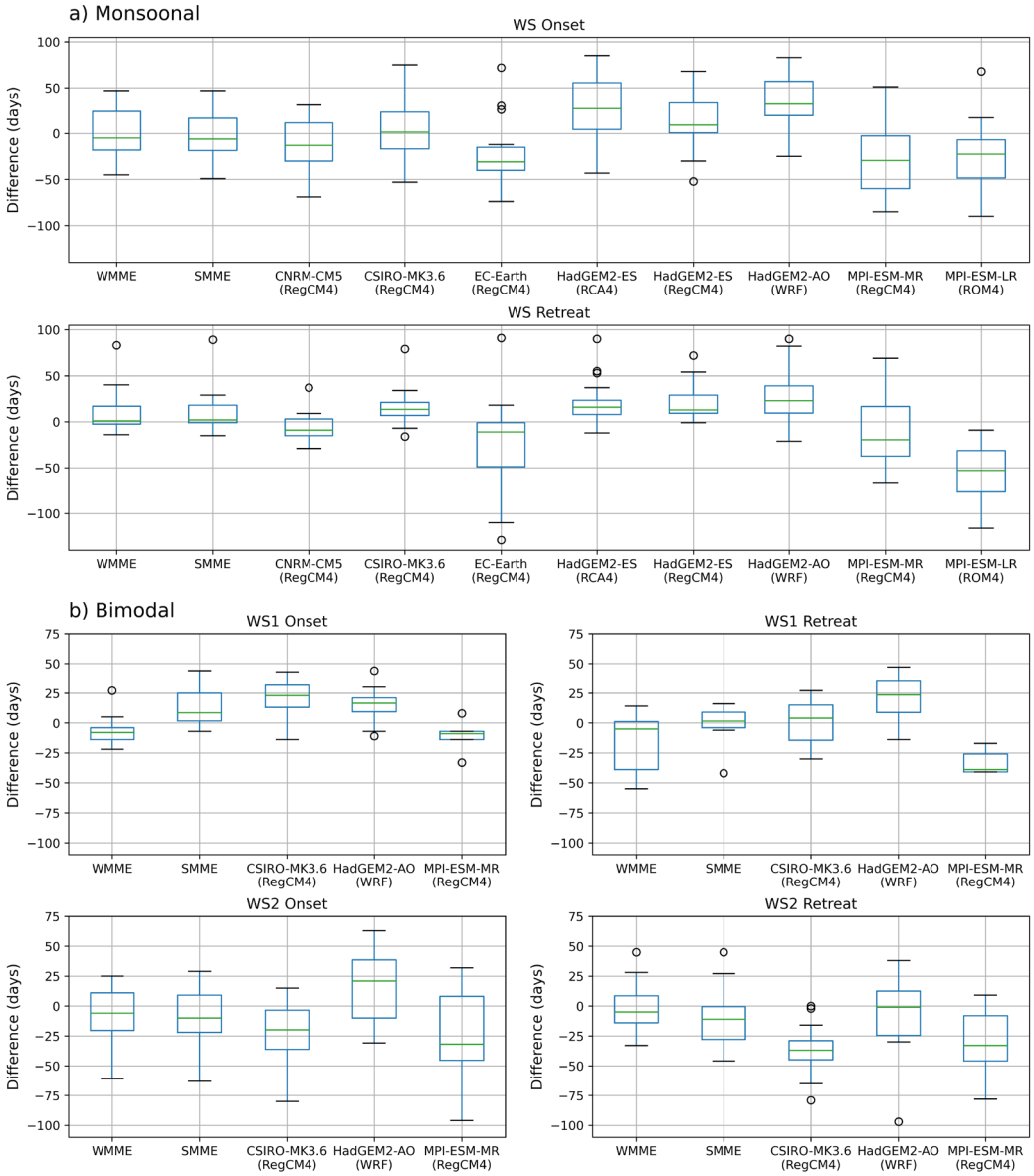

Figure 10. Boxplot of interannual WS timing differences between models and observation for regions a) monsoonal and b) bimodal.

The distribution of the difference between the onset and retreat of the annual WS between models and observation is shown in a boxplot in Figure 10. Zero value mean model and observation have the same timing. In the monsoonal region (Fig. 10a), the two MMEs produced similar distributions of WS onset differences and were closer to observation than the individual models. The distribution of WMME has first quartile (Q1), median (Q2), and minimum values that are closer to zero than SMME, but SMME has better upper quartile (Q3) values. A similar distribution was also obtained for the WS retreat, with SMME having a slightly higher outlier value than WMME.

Differences in the annual mean of onset, retreat, duration, and SDII of WS of all models with observation in the monsoonal region can be seen in Figure 11. The annual mean of WS onset occurred earlier in all models compared to observation, except CSIRO-MK3.6 (RegCM4) and the entire HadGEM2 model. The annual mean of WS retreat was simulated late by most models, except CNRM-CM5 (RegCM4), EC-Earth (RegCM4), and all MPI models. The simulated annual mean of WS duration was longer by most of the models, except HadGEM2-ES (RCA4), HadGEM2-AO (WRF), and MPI-ESM-LR (ROM4). All models produce an annual SDII mean higher than the observation, except MPI-ESM-LR (ROM4). All MMEs, resulting in similar WS timing, are closer to observation than all individual models. WMME performs best with its WS onset two days closer to observation than SMME.

In bimodal regions, observation data shows that the annual average of WS1 ranges from March 13 to May

16, with a duration of 64 days and an SDII of 9.59 mm/day. The WS2, on annual average, lasts for 114 days, from October 1 to January 23, with 9.7 mm/day SDII. The difference in WS timing, duration, and SDII between the models and observation in the bimodal regions is shown in Figure 10b. WMME has the smallest bias in simulating observation WS1 onset, mostly earlier than the observation. The retreat of WS1 by SMME is most similar to observation compared to other models. The two MMEs produce similar annual bias distribution of observation WS2 onset and are better than all individual models, with WMME slightly performing better. The annual WS2 retreat simulated by WMME has a closer value with observation than other models.

The annual mean differences in the WS timing, duration, and SDII of all models with observation in the bimodal regions can be seen in Figure 12. At WS1, WMME produces the annual mean of onset and duration closest to the observation. CSIRO-MK3.6 (RegCM4) shows the same annual mean of WS1 retreat with observation. In simulating the annual average of WS2 timing, most models result in retreat WS2 with a shorter duration than observation. Compared to observation, SMME can produce the same WS2 duration but with an earlier start of nine days. However, WMME produces closer WS2 timing to observation than SMME. All models' annual mean SDII at WS1 and WS2 is higher than the observation, with WMME being the closest.

The categorizing of rainfall seasonal patterns using corrected CHIRPS data generally agrees with several previous studies [6], [7], with monsoonal patterns in most parts of Indonesia. Most models can simulate monsoonal patterns, in which two monsoon systems influence their seasonal cycle [7]. This result aligns with Tangang et al. [5], which state that the CORDEX-SEA model can simulate the monsoon system and the rainfall movement well. The anti-monsoonal patterns are generally found in areas with small islands, such as Maluku. The inability of the model to simulate these anti-monsoonal patterns agrees with Tangang et al. [5], who stated the lack of model ability to simulate annual rainfall in areas with many islands.

In the monsoonal regions, the WS onset simulated by CORDEX-SEA WMME occurred earlier than the observation. This result aligns with research by Hariadi et al. [21], which showed season onset of the CORDEX model is earlier than the observation in most of the areas in this study that had a monsoonal pattern.

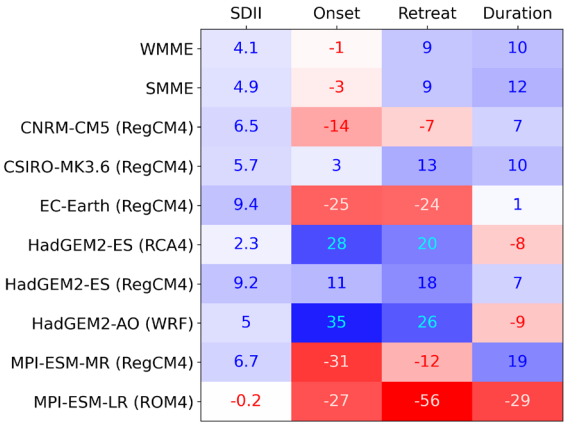

Figure 11. Difference of WS annual mean between the model and observation in the monsoonal regions. Onset, retreat, and duration (SDII) are shown in days (mm/day).

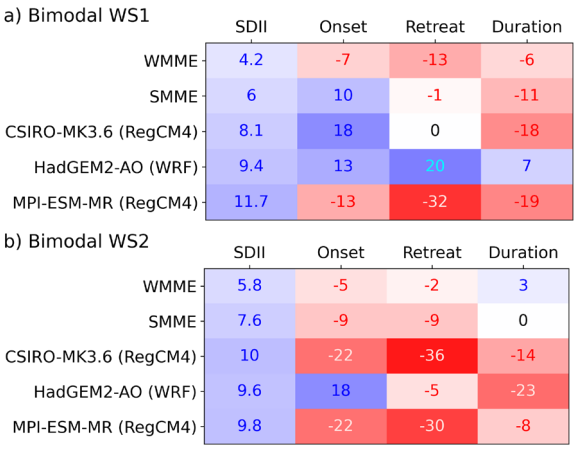

Figure 12. Same as Figure 11, but for the bimodal regions at a) WS1 and b) WS2.

Research by Tangang et al. [5] stated that the CORDEX-SEA models with RCMs of RegCM4 and WRF have a wet bias, while RCA4 and ROM have a dry bias. Consistent with that, Juneng et al. [35] also stated that RegCM4 produces wetter simulations. That statements agree with the results of this study, which is that most of the individual models produce a wet bias, except for MPI-ESM-LR (ROM4) with a dry bias. In the HadGEM2-ES (RCA4) model, the difference in bias with the result of Tangang et al. [5] may be due to the different time coverage, whereas this study only calculates SDII during WS. As most of the individual models in this study used RegCM4, which has a wet bias, the ensemble process that was carried out still shows a wet bias. However, weighted ensembles have a lower wet bias than most individual models.

4. Conclusion

Corrections of CHIRPS daily rainfall data using BMKG blended *dasarian* rainfall data can produce seasonal rainfall patterns that align with in situ observations. The seasonal rainfall patterns generated by the individual CORDEX-SEA simulation models have different spatial distributions in most parts of Indonesia. However, they are generally the same throughout the southern part of Indonesia, including Lampung, Java, Bali, NTT, and the southern part of Papua. The spatial distribution of the seasonal rainfall patterns of WMME and SMME tends to be similar except in Kalimantan and Papua. The models best describe the monsoonal pattern, while the anti-monsoonal pattern is the most difficult to simulate. The agreement of the seasonal pattern of the MMEs with observation is better than individual models, with the WMME outperforming the SMME.

From climatological values, in monsoonal and bimodal regions, all MMEs models produce WS timing and SDII closer to observation than individual models. Although only slightly different, WMME is better than SMME. In the anti-monsoonal regions, only two models, CNRM-CM5 (RegCM4) and EC-Earth (RegCM4), produced a pattern like the observation but with significantly different climatological WS timing.

Based on the annual WS, the onset and retreat of WS from the MMEs tend to occur around its annual mean value. So, it is hard to simulate the annual variation of observation WS timing, including in years with extreme events such as the strong El Nino in 1997-1998. MMEs perform better than individual models in simulating the observation annual average of WS timing, duration, and SDII.

In general, WMME has the best performance compared to SMME and individual models in simulating the characteristics of WS in Indonesia. In monsoonal and bimodal regions, compared with SMME and individual models, the weighting process on WMME can reduce rainfall bias and make the simulated WS onset and duration closer to observation values, except for the retreat of the WS which still varies. However, all models cannot simulate seasonal rainfall patterns in anti-monsoonal regions.

References

[1] LQ Avia, “Change in rainfall per-decades over Java Island, Indonesia,” *IOP Conf. Ser. Earth Environment. sci.* , vol. 374, no. 1, p. 012037, Nov. 2019, doi: 10.1088/1755-1315/374/1/012037.

[2] N. Herlina and A. Prasetyorini, "Effect of Climate Change on Planting Season and Productivity of Maize (Zea mays L.) in Malang Regency," *J. Agricultural Science. Indonesia.* , vol. 25, no. 1, pp. 118–128, Jan. 2020, doi: 10.18343/jipi.25.1.118.

[3] AB Sekaranom, E. Nurjani, and F. Nucifera, “Agricultural Climate Change Adaptation in Kebumen, Central Java, Indonesia,” *Sustainability* , vol. 13, no. 13, p. 7069, Jun. 2021, doi: 10.3390/su13137069.

[4] RL Naylor, DS Battisti, DJ Vimont, WP Falcon, and MB Burke, “Assessing risks of climate variability and climate change for Indonesian rice agriculture,” *Proc. Christmas. Acad. sci.* , vol. 104, no. 19, pp. 7752–7757, May 2007, doi: 10.1073/pnas.0701825104.

[5] F. Tangang *et al.* , “Projected future changes in rainfall in Southeast Asia based on CORDEX–SEA multi-model simulations,” *Clim. Dyn.* , vol. 55, no. 5–6, pp. 1247–1267, Sept. 2020, doi: 10.1007/s00382-020-05322-2.

[6] J. -I. Hamada, MD Yamanaka, J. Matsumoto, S. Fukao, PA Winarso, and T. Sribimawati, “Spatial and Temporal Variations of the Rainy Season over Indonesia and their Link to ENSO.,” J. Meteorol . *Soc. jpn. Ser II* , vol. 80, no. 2, pp. 285–310, 2002, doi: 10.2151/jmsj.80.285.

[7] E. Aldrian and R. Dwi Susanto, "Identification of three dominant rainfall regions within Indonesia and their relationship to sea surface temperature," *Int. J. Climatol.* , vol. 23, no. 12, p. 1435–1452, Oct. 2003, doi: 10.1002/joc.950.

[8] B. Liebmann *et al.* , “Seasonality of African Precipitation from 1996 to 2009,” *J. Clim.* , vol. 25, no. 12, p. 4304–4322, Jun. 2012, doi: 10.1175/JCLI-D-11-00157.1.

[9] CM Dunning, ECL Black, and RP Allan, “The onset and cessation of seasonal rainfall over Africa,” *J. Geophys. Res. Atmospheres* , vol. 121, no. 19, Oct. 2016, doi: 10.1002/2016JD025428.

[10] CM Dunning, E. Black, and RP Allan, “Later Wet Seasons with More Intense Rainfall over Africa under Future Climate Change,” *J. Clim.* , vol. 31, no. 23, pp. 9719–9738, Dec. 2018, doi: 10.1175/JCLI-D-18-0102.1.

[11] B. Wang *et al.* , “Monsoons Climate Change Assessment,” *Bull. Am. meteorol. Soc.* , vol. 102, no. 1, pp. E1–E19, Jan. 2021, doi: 10.1175/BAMS-D-19-0335.1.

[12] G. Nikulin *et al.* , “The effects of 1.5 and 2 degrees of global warming on Africa in the CORDEX ensemble,” *Environ. Res. Lett.* , vol. 13, no. 6, p. 065003, May 2018, doi: 10.1088/1748-9326/aab1b1.

[13] F. Ge *et al.* , “Risks of precipitation extremes over Southeast Asia: does 1.5 °C or 2 °C global warming make a difference?,” *Environ. Res. Lett.* , vol. 14, no. 4, p. 044015, Apr. 2019, doi: 10.1088/1748-9326/aaff7e.

[14] Supari *et al.* , “Multi-model projections of precipitation extremes in Southeast Asia based on CORDEX-Southeast Asia simulations,” *Environ. Res.* , vol. 184, p. 109350, May 2020, doi: 10.1016/j.envres.2020.109350.

[15] M. Herrmann, T. Nguyen-Duy, T. Ngo-Duc, and F. Tangang, “Climate change impact on sea surface winds in Southeast Asia,” *Int. J. Climatol.* , vol. 42, no. 7, pp. 3571–3595, 2022, doi: https://doi.org/10.1002/joc.7433.

[16] SI Seneviratne *et al.* , “Changes in Climate Extremes and their Impacts on the Natural Physical Environment,” in *Managing the Risks of Extreme Events and Disasters to Advance Climate Change Adaptation: Special Report of the Intergovernmental Panel on Climate Change* , CB Field, Q. Dahe, TF Stocker , and V. Barros, Eds. Cambridge: Cambridge University Press, 2012, pp. 109–230. doi: 10.1017/CBO9781139177245.006.

[17] E. -S. Im, Y. -W. Choi, and J. -B. Ahn, "Robust intensification of hydroclimatic intensity over East Asia from multi-model ensemble regional projections," *Theor. appl. climatol.* , vol. 129, no. 3–4, pp. 1241–1254, Aug. 2017, doi: 10.1007/s00704-016-1846-2.

[18] N. Herger, G. Abramowitz, R. Knutti, O. Angélil, K. Lehmann, and BM Sanderson, “Selecting a climate model subset to optimize key ensemble properties,” *Earth Syst. Dyn.* , vol. 9, no. 1, pp. 135–151, Feb. 2018, doi: 10.5194/esd-9-135-2018.

[19] C. Miao, Q. Duan, Q. Sun, and J. Li, “Evaluation and application of Bayesian multi-model estimation in temperature simulations,” *Prog. Phys. geogr. Earth Environment.* , vol. 37, no. 6, pp. 727–744, Dec. 2013, doi: 10.1177/0309133313494961.

[20] D. Nohara, A. Kitoh, M. Hosaka, and T. Oki, “Impact of Climate Change on River Discharge Projected by Multimodel Ensemble,” *J. Hydrometeorol.* , vol. 7, no. 5, pp. 1076–1089, Oct. 2006, doi: 10.1175/JHM531.1.

[21] WS Hariadi *et al.* , “Evaluation of onset, cessation and seasonal precipitation of the Southeast Asia rainy season in CMIP5 regional climate models and HIGHRESMIP global climate models,” *Int. J. Climatol.* , vol. 42, no. 5, pp. 3007–3024, Apr. 2022, doi: 10.1002/joc.7404.

[22] M. Collins *et al.* , “Long-term climate change: Projections, commitments and irreversibility,” in *Climate Change 2013: The Physical Science Basis. Contribution of Working Group I to the Fifth Assessment Report of the Intergovernmental Panel on Climate Change* , TF Stocker, D. Qin, G.-K. Plattner, M. Tignor, SK Allen, J. Doschung, A. Nauels, Y. Xia, V. Bex, and PM Midgley, Eds. Cambridge, UK: Cambridge University Press, 2013, pp. 1029–1136. doi: 10.1017/CBO9781107415324.024.

[23] C. Funk *et al.* , “The climate hazards infrared precipitation with stations—a new environmental record for monitoring extremes,” *Sci. Data* , vol. 2, no. 1, p. 150066, Dec. 2015, doi: 10.1038/sdata.2015.66.

[24] Supari, F. Tangang, L. Juneng, and E. Aldrian, “Observed changes in extreme temperature and precipitation over Indonesia: EXTREME TEMPERATURE AND PRECIPITATION OVER INDONESIA,” *Int. J. Climatol.* , vol. 37, no. 4, pp. 1979–1997, Mar. 2017, doi: 10.1002/joc.4829.

[25] F. Giorgi *et al.* , “RegCM4: model description and preliminary tests over multiple CORDEX domains,” *Clim. Res.* , vol. 52, pp. 7–29, Mar. 2012, doi: 10.3354/cr01018.

[26] J. Michalakes *et al.* , “THE WEATHER RESEARCH AND FORECAST MODEL: SOFTWARE ARCHITECTURE AND PERFORMANCE,” in *Use of High Performance Computing in Meteorology* , Reading, UK, Sep. 2005, pp. 156–168. doi: 10.1142/9789812701831_0012.

[27] G. Strandberg *et al.* , “CORDEX scenarios for Europe from the Rossby Center regional climate model RCA4,” *SMHI* , vol. 116, 2014.

[28] DV Sein *et al.* , “Regionally coupled atmosphere-ocean-sea ice-marine biogeochemistry model ROM: 1. Description and validation,” *J. Adv. Model. Earth System.* , vol. 7, no. 1, pp. 268–304, Mar. 2015, doi: 10.1002/2014MS000357.

[29] KE Taylor, “Summarizing multiple aspects of model performance in a single diagram,” *J. Geophys. Res. Atmospheres* , vol. 106, no. D7, pp. 7183–7192, Apr. 2001, doi: 10.1029/2000JD900719.

[30] X. Yang *et al.* , “The Optimal Multimodel Ensemble of Bias-Corrected CMIP5 Climate Models over China,” *J.*

Hydrometeorol. , vol. 21, no. 4, pp. 845–863, Apr. 2020, doi: 10.1175/JHM-D-19-0141.1.

[31] RPD Walsh and DM Lawler, "RAINFALL SEASONALITY: DESCRIPTION, SPATIAL PATTERNS AND CHANGE THROUGH TIME," *Weather* , vol. 36, no. 7, pp. 201–208, Jul. 1981, doi: 10.1002/j.1477-8696.1981.tb05400.x.

[32] T. Peterson, "Climate change indices," *WMO Bull.* , vol. 54, no. 2, pp. 83–86, 2005.

[33] Y. Darmawan, H.-H. Hsu, and J. -Y. Yu, "Characteristics of Large-Scale Circulation Affecting the Inter-Annual Precipitation Variability in Northern Sumatra Island during Boreal Summer," *Atmosphere* , vol. 12, no. 2, 2021, doi: 10.3390/atmos12020136.

[34] R. Knutti, R. Furrer, C. Tebaldi, J. Cermak, and GA Meehl, "Challenges in Combining Projections from Multiple Climate Models," *J. Clim.* , vol. 23, no. 10, p. 2739–2758, 2010, doi: 10.1175/2009JCLI3361.1.

[35] L. Juneng *et al.* , "Sensitivity of Southeast Asia rainfall simulations to cumulus and air-sea flux parameterizations in RegCM4," *Clim. Res.* , vol. 69, no. 1, pp. 59–77, Jun. 2016, doi: 10.3354/cr01386.